UNDERWATER ROBOT FOR TUNNEL INSPECTION: DESIGN AND CONTROL

Rodrigo F. Carneiro, Antonio C. Leite, Alessandro J. Peixoto, Christiano Goulart, Ramon R. Costa, Fernando Lizarralde and Liu Hsu *

* *Department of Electrical Engineering - COPPE*
Federal University of Rio de Janeiro
Rio de Janeiro, Brazil

Email: [rodrigo, toni, jacoud, chris, ramon, fernando, liu]@coep.ufrj.br

Abstract— This work presents a new design concept for a remotely operated vehicle aimed to perform inspection tasks in flooded tunnels and dams. Depth and yaw controllers were developed to regulate the vehicle position in front of target area in the wall. Video cameras and sonar are used to detect disruptions in the walls or accumulated debris. Experimental results are presented to illustrate the performance and viability of the proposed controllers.

Keywords— Mobile Robots, Underwater Robots, Remote Control, Teleoperation.

Resumo— Neste trabalho apresenta-se um projeto conceitual de um veiculo de operação remota para inspeção de barragens e túneis de adução. O controle de rumo e de profundidade foi desenvolvido para regular a posição do veículo em frente a parede de interesse. Câmeras de vídeo e sonares são usados para localizar danos nas paredes ou detritos acumulados. Resultados experimentais são apresentados para ilustrar o desempenho e a viabilidade dos controladores propostos.

Palavras-chave— Robôs Móveis, Robôs Submarinos, Controle Remoto, Teleoperação.

1 Introduction

In recent years, there is a growing necessity of executing several tasks with efficiency and accuracy in environments where the human presence is very difficult, hazardous or even impossible. In this framework, the visual inspection of flooded tunnels in hydroelectric facilities has been performed in order to detect disruptions in the tunnel walls and check the presence of accumulated debris. At first, this task should be executed by direct inspection inside the tunnel after the water has been completely removed. However, the dewatering process is a slow and unsafe operation. The dewatering must be carefully controlled to avoid the increase of groundwater pressure on the tunnel wall. If the tunnel emptying is too fast it can also cause landslide at the dam site. An alternative solution is the use of remotely operated vehicles (ROVs) to execute underwater inspection tasks. Most of the benefits derived from remote inspections are due to dewatering avoidance and safety operation from the control station.

The utilization of ROVs to inspect hydraulic tunnels is not a new idea. The first attempts were performed in the early 80s. Nowadays, there are several companies which are devoted for this type of operation as well as ROVs specifically designed for this aim (Clarke, 2002; Marty, 2003). In spite of the advances already obtained in the ROVs development, the usage of this technology to execute tasks inside tunnels still has some problems. In contrast with tasks accomplished offshore, where the ROVs and their cages are placed near to the workplace, the tunnel inspection requires the displacement of the ROV by long distances in the horizontal direction. As integral part of the vehicle, the umbilical cable should be appropriately designed for the mission as well as the maximum forward thrust of the vehicle which should be enough to allow the ROV to drag the cable inward the tunnel. Moreover, the poor quality of the water inside the tunnel can generate low visibility due to the high density of suspended particles, mainly in the rain period. The incident light rays which strike the particles are reflected causing the *back-scattering* phenomenon, that is difficult to deal with. Therefore, the usual methods to lighten the environment, similar to those employed in offshore applications, do not allow the acquisition of sufficiently clear images.

This work addresses the problem of designing an ROV system for pipelines, tunnels and dams inspections under low visibility conditions.

2 Design concept

In order to overcome the difficulties presented in tunnel inspection missions, a new design concept for an ROV is proposed. The main features of this ROV are the following:

- Battery system to eliminate the necessity of power lines within the umbilical cable;
- Four thrusters to allow positioning and heading control of the ROV;
- Underwater lighting system based on high luminous intensity and low consumption LEDs;
- Communication link between the ROV and the console station through a single fiber optic cable;
- On-board launch-and-recovery mechanism for the fiber optic cable in order to avoid the problem of dragging the cable inside the tunnel;
- Adjustable buoyancy system for depth control assistance;
- The adjustable buoyancy system must automatically compensate and correct the depth of the ROV accordingly as the cable has been launched or recovered;
- The outer frame of the ROV must have no sharp borders in order to make easier its recovery by pulling the cable in case of failure;

- The navigation system employs an inertial measurement unit (IMU), two ultrasound altimeters for underwater distance measurements and a pressure sensor for depth measurement;
- The inspection system is composed by one color video camera, three black & white cameras, one high sensitivity (SIT) camera and one profiling sonar.

This design embodies some of the components already used in ROVs specifically designed to operate inside tunnels, as described in literature. The use of on-board batteries and communication through a single fiber optic cable were inspired by the Tunnel Sea Lion ROV (TSL) (Aggev et al., 2000). The TSL has a system that freely releases the fiber optic while the ROV moves forward. The video cameras and sonar configuration is similar to the one employed by ASI Mantaro ROV (Clarke, 2002).

In the proposed system, a servomechanism drives a reel that releases and recovers the fiber optic cable as the ROV moves inside the tunnel. The variation of the ROV buoyancy, due to the cable handling, is compensated by the *adjustable buoyancy system*. One innovation introduced in this ROV design is the application of *high luminous intensity LEDs* for underwater lighting (patent pending). Notice that both, the adjustable buoyancy system and LED lighting, are necessary in order to minimize the energy consumption for the ROV operation and, hence, the mass of batteries.

3 Technical overview

This section presents some additional technical details about the proposed ROV, henceforth named as LUMA, and its design and operation modes.

3.1 General vehicle design

The main vehicle dimensions and specifications are:

Dry weight	40 kg
Length	1 m
Width	0.85 m
Height	0.65 m
Max Speed	2 m/s
Max Depth	70 m
Endurance	8 hours
Max length of fiber optical cable	1 km

Figure 1 shows a view of a CAD representation of LUMA where some of the main components can be identified.

3.2 Battery and power management

A set of two 72 VDC and 20 Ah, high energy density, ion-lithium battery packs powers the propulsion. LUMA also has a set of DC/DC converters to reduce the voltage for instruments and all electronic circuits. This set of batteries allows 8 hours of continuous operation.

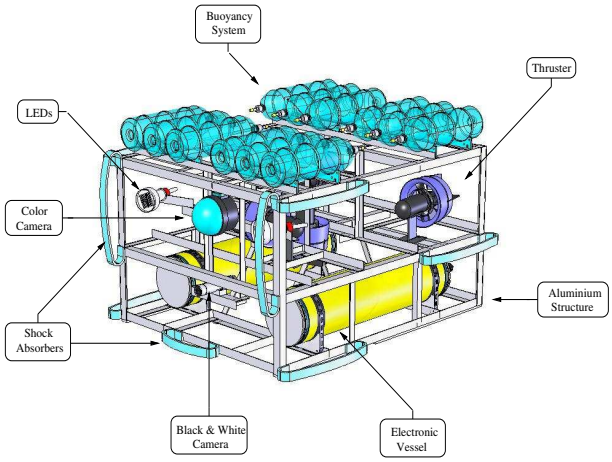

Figure 1: LUMA ROV and its main components.

3.3 Propulsion

The vehicle propulsion system is composed by four thrusters (1 hp each): two of them installed along the longitudinal direction, one along the transversal and other along the vertical direction. The proper combination of the thrusters allows a 4-DOF motion. Each thruster (motor + propeller) is equipped with an encoder and an internal driver commanded by an analog signal.

3.4 Video system

The video system is composed by five video cameras as follow:

- One high resolution black & white camera provides wide angle forward vision for navigation;
- One high resolution color camera, with pan and tilt, allows detailed inspection of the area being surveyed under high visibility conditions (low level of suspension particles);
- One high resolution and high sensitivity camera (SIT camera) for inspection under low light level and medium visibility conditions;
- Two auxiliary low resolution black & white video cameras for surveillance of the equipment and aid in precision maneuvers.

3.5 Communication system

A fiber optic cable provides the command-data link between LUMA control system and the operator console. Figure 2 illustrates the TTL/RS-485 and RS-485/USB converters required at each end of the link.

Video is transmitted from the ROV to the console in half-duplex mode. The communication of commands and telemetry data signals requires a full-duplex mode.

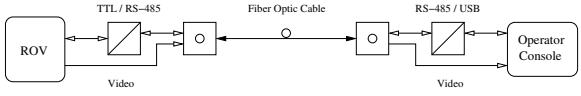

Figure 2: Block diagram of the communication link.

3.6 Navigation

The navigation system consists of an inertial measurement unit 3DM-G (MicroStrain, Inc.), a submersible pressure sensor WL400 (Global Water, Inc.) and a digital precision altimeter PA200 (Tritech Ltd.). The IMU combines information from gyros, magnetometers and accelerometers to output its orientation in dynamic and static environments. However, only the yaw angle is used for feedback. The pressure sensor is used to monitor and control the LUMA depth (pressure is easily converted into depth through a conversion factor), while the altimeter is used to control the LUMA position with respect to the wall of interest.

3.7 Control system and supervision

LUMA control system consists of an operator console, which includes a PC computer, joystick and a communication device. The operator console is intended for input of control information and LUMA operation mode by a graphic user interface (GUI) and also for visualization of sensors data.

The GUI is designed as one-window interface based on C++ language which allows the control of LUMA motion parameters and data visualization from IMU, cameras, depth sensor, sonars and log. GUI also enables to switch on/off modes of program control system operation, extended data set visualization, alarms indication and LUMA testing.

3.8 Teleoperation system

LUMA was developed for remote teleoperation by a force feedback joystick. The acquired data are analyzed by an operator who takes decisions according to the mission and sends commands to the ROV control system through the joystick. The control system supplies each thruster with a velocity signal in order to place the ROV at the target position. For a proper inspection, an automatic orientation (yaw) and depth control algorithms are used.

4 System Modeling

This section presents the detailed ROV modeling. The following topics are addressed: coordinates systems, motion equations and thrusters modeling.

4.1 Coordinates systems

The coordinates systems used in the modeling of ROV dynamics are the body frame attached in the ROV and the inertial frame, as shown in Figure 3. The ROV attitude is given by a set of ZYX Euler angles, also called Roll-Pitch-Yaw angles, denoted by ϕ, θ and ψ, respectively. In this case, the triplet of angles $[\,\phi \;\; \theta \;\; \psi\,]^T$ represents rotations defined with respect to a fixed frame attached to the center of mass of the vehicle.

4.2 Motion equations

In robotic literature several models for an ROV have been proposed. The model developed in (Cunha et al., 1991) is a sufficiently-complete research among already published works.

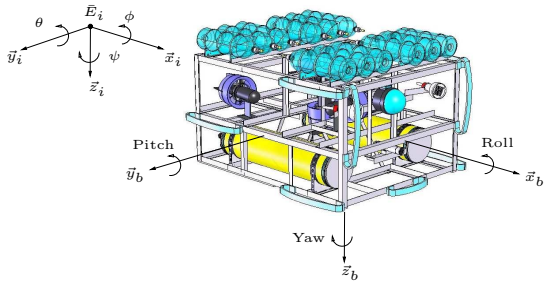

Figure 3: ROV and coordinates systems.

The considered model, which assumes that the water current velocity is constant, is given by

$$\begin{bmatrix} \dot{U} \\ \dot{\Omega} \end{bmatrix} = I_{ma}^{-1} \begin{bmatrix} F_H + F_{GB} + F_T + F_C + F_I \\ M_H + M_{GB} + M_T + M_C + M_I \end{bmatrix}, \tag{1}$$

where U and Ω are the translational and rotational velocities of the ROV represented in the body frame; I_{ma} is the inertia matrix. Note that, the forces and moments that acts in the ROV are denoted by the following subscripts: hydrodynamic (H), gravity and buoyancy (GB), thrusters (T), umbilical cable (C) and inertial (I). Hydrodynamics parameters are identified as in (Avila, 2004).

4.3 Thrusters modeling

A precise model for the thruster is necessary in order to determine the total force and moment generated by the vectorial combination of all thruster. In the static model adopted in (Cunha et al., 1991), the counterflow F_{ti} and the axial moment M_{ti} produced by each thruster are given by

$$F_{ti} = C_T^*(\sigma)\,\frac{\rho}{8}\,[v_{wi}^2 + (0.7\,\pi\,n_{ti}\,D_p)^2]\,\pi\,D_p^2\,, \tag{2}$$

$$M_{ti} = C_Q^*(\sigma)\,\frac{\rho}{8}\,[v_{wi}^2 + (0.7\,\pi\,n_{ti}\,D_p)^2]\,\pi\,D_p^3\,, \tag{3}$$

where n_{ti} is the propeller rotation velocity of the i-th thruster [rps], D_p is the propeller diameter [m], v_{wi} is the water velocity that enters into the propeller disc of the i-th thruster [m/s] and ρ is the specific mass of water [kg/m^3]. The parameters $C_T^*(\sigma)$ and $C_Q^*(\sigma)$ can be calculated by

$$C_T^* = \frac{8\,F_{t,max}}{0,7\,\rho\,\pi^3\,n_{t,max}^2\,D_p^4}\,, \quad C_Q^* = \frac{8\,M_{t,max}}{0,7\,\rho\,\pi^3\,n_{t,max}^2\,D_p^5}\,,$$

where $F_{t,max}$ and $M_{t,max}$ are obtained when the thruster rotation assumes a maximum value represented by $n_{t,max}$. Then, the total thrusters contribution is described by

$$F_T = \sum_{i=1}^{n} F_{ti}\,P_{ti}\,, \tag{4}$$

$$M_T = \sum_{i=1}^{n} [M_{ti}\,P_{ti} + R_{ti} \times (F_{ti}\,P_{ti})]\,, \tag{5}$$

where n is the number of thrusters, R_{ti} and P_{ti} describe the propeller counterflow center and the propeller counterflow direction of the i-th thruster, respectively, under the following assumptions:

- the crossed coupling due to the water flow interference among thrusters is negligible;
- v_{wi} was assumed to be the relative velocity of the vehicle that is parallel to the propeller rotation axis of the i-th thruster;
- the inertia of the thrusters is negligible.

5 Control Design

In the section, some simplifications are adopted to make easier the control design. The following topics are addressed: compensators, simplified model for ROV dynamics and controller design.

5.1 Compensators

In order to linearize the thrusters response, two compensators were included at the input of each thruster: a static compensator and a dead-zone compensator. The static compensator counterbalances the quadratic nonlinearity and the dead-zone compensator is used to minimize the dead-zone effect of thrusters. The following static compensator is used

$$\bar{n}_{ti} = sgn(\bar{F}_{ti}\,\alpha_i^+)\sqrt{\frac{|\bar{F}_{ti}|}{|\alpha_i^*|}}\,, \tag{6}$$

where $\bar{F}_{ti}$ is the command signal (i.e., counterflow) of the i-th thruster and

$$\alpha_i^* = \begin{cases} \alpha_i^+ = \quad C_T^*(0)\,\frac{\rho}{8}\,0.7^2\,\pi^3\,D_p^4\,, & sgn(\bar{F}_{ti}\,\alpha_i^+) \geq 0\,, \\ \alpha_i^- = -C_T^*(\pi)\,\frac{\rho}{8}\,0.7^2\,\pi^3\,D_p^4\,, & sgn(\bar{F}_{ti}\,\alpha_i^+) < 0\,. \end{cases}$$

Thrusters motors turn on only if they are supplied with a larger voltage than a minimum value u_{min}. Then, a dead-zone compensator is given by

$$\bar{u}_{ti} = \begin{cases} \bar{n}_{ti} + u_{min}\,, & \bar{n}_{ti} > 0\,, \\ \bar{n}_{ti} - u_{min}\,, & \bar{n}_{ti} < 0\,, \end{cases} \tag{7}$$

where $\bar{u}_{ti}$ is the supply voltage of the i-th thruster; $\bar{n}_{ti}$ is the reference voltage of static compensator of the i-th thruster.

5.2 Simplified model for ROV dynamics

The yaw dynamics is activated by 4 thrusters. However, as verified experimentally, the vertical thruster $T1$ can be neglected in the adopted model for the controller design, since it almost does not affect the ROV's yaw. Thus, the yaw dynamics is governed only by thrusters $T2$, $T3$ and $T4$. As a result, the system can be modeled by a multivariable system with 3 inputs and 1 output (MISO). However, by using a proper decoupling matrix D, in order to control each DOF separately, it is possible to simplify the modeling of yaw dynamics, resulting in a SISO system as shown in Figure 4.

According to the model, the system has 1 input given by moment M_z around the z-axis and 1 output being the yaw angle ψ. Note that, F_x and F_y are the resulting desired forces in the axes x and y of the body frame. Neglecting the hydrodynamic friction, the following yaw dynamic model can be used

$$\ddot{\psi}(t) = k\,M_z(t)\,, \tag{8}$$

where k denotes the high frequency gain. This gain can be identified by using the Relay Feedback Method (Astrom and Hagglund, 1984).

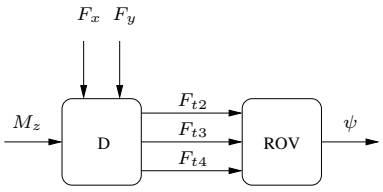

Figure 4: SISO model for ROV yaw dynamics.

5.3 Control modes

The command signals are sent to the ROV by the joystick according to the following operation modes:

- **Manual**: The values corresponding to axes 1, 2, 3 and 4 of the joystick denote the quadruple $[\,F_x\ F_y\ M_z\ F_z]^T$ respectively, where F_x is the resulting of desired force in the x-axis of the frame attached in ROV (analogously to F_y and F_z) and M_z is the resulting moment around the z-axis. In this mode, the ROV is open-loop commanded.
- **Automatic Depth**: This mode is activated as soon as the *automatic depth* command is sent to LUMA. In this moment the current value of depth is maintained by a closed-loop control. The depth is measured by the pressure sensor described above which provides a DC current into the range $4-20$ [mA] representing $0-76.2$ [m] respectively.
- **Automatic Yaw**: This mode is activated as soon as the *automatic yaw* command is sent to LUMA. In this moment the current value of yaw angle is maintained by a closed-loop control. The yaw angle is measured by IMU which provides a digital word into the range $[-32768,\ 32767]$ representing $[-180,\ 180]$ degree, respectively.

5.4 P-PI controller

According to previous works (Cunha et al., 1991), one selects the P-PI usual linear controller due to simplicity in implementation, familiarity with the controller structure, facility in control design and possibility for *in-loco* tuning. The P-PI controller is composed by two feedback loops (Russel, 1984): a proportional plus integral velocity feedback (slave loop) and a proportional position feedback (master loop).

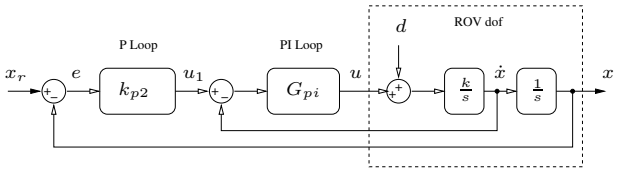

Figure 5: P-PI controller.

Figure 5 shows the P-PI control scheme applied to a generic DOF (x) of the ROV. The gain adjustment of the controller is based on pole-placement technique. However, the poles cannot be arbitrarily chosen (this could result in a very fast dynamic response) due to several simplifications adopted in the dynamic model

of the considered DOF. (e.g., the thruster is only modeled for its static response)

For this reason, the gain adjustment is based on two steps (Cunha et al., 1991): First, one adjusts the velocity control loop (internal loop) followed by the adjustment of the position control loop (external loop). To make the adjustment of the internal loop (PI), one opens the external loop (P) and calculates the gains k_{p1} and k_i in order to obtain double poles. These poles are placed on $s = bc$, where b is the P-PI dominant pole and $c > 1$ is a constant[1].

>From the characteristic equation of the internal loop $s^2 + k\,k_{p1}\,s + k\,k_i = 0$, one obtains the following gains

$$k_{p1} = -\frac{2cb}{k}, \quad k_i = \frac{(cb)^2}{k}, \tag{9}$$

where k is the *high frequency gain*. The external loop is adjusted in order to force the characteristic equation of the system with both loops

$$s^3 - 2cbs^2 + (c^2b^2 - 2cbk_{p2})s + (cb)^2 k_{p2} = 0, \tag{10}$$

to have a root located on $s = b$ (i.e., dominant pole). Thus, the gain k_{p2} is calculated by the following equation

$$k_{p2} = \frac{b(2c - c^2 - 1)}{c(c-2)}. \tag{11}$$

In the second step, since the poles cannot be arbitrarily placed, it is necessary to validate the control design by simulation or experimental tests with the ROV. The algorithm for iterative tuning of P-PI controller is described as follows. First, the controllers are independently tuned, one at a time. To achieve this aim, several simulations (or experiments) are performed. The gains are calculated by (9) and (11), where $c = 3$ shown to be a reasonable value. The initial condition for each simulation is chosen to excite predominantly the yaw dynamic. The others initial conditions are null. The controller is tuned iteratively starting with a large initial time constant ($1/|b|$), which is slowly reduced in consecutive simulations. The iterative process is finished when the settling time is minimal and no overshoot is apparent.

Remark 1 *The P-PI controller requires ROV velocity ($\dot{x}$), which is not measured directly. Velocity could be measured by additional transducers. However, this would increase cost. An alternative is to use velocity estimation from position measurement (x). Here, the classical solution is adopted: each velocity coordinate is estimated by a first-order lead filter with transfer function $L(s) = s/(\tau s + 1)$, where τ is a design parameter.*

Remark 2 *According to (Russel, 1984), one has to saturate the internal loop reference velocity (u_1) in order to limit the maximum velocity of ROV (v_{max}) when the operator requires wide movements. This improves the controller performance despite the ROV velocity limitation.*

[1]The symbol "s" represents the Laplace variable.

5.5 Anti-reset windup strategy

In order to avoid problems due to the thrusters saturation, it is necessary to employ the well-known anti-reset windup (ARW) strategy for the P-PI controller (Astrom and Wittenmark, 1997). Here, one adopts to limit the controller output and stop the integral action as soon as the integrator state get out of the range $[-1,\ 1]$. A block diagram of a P-PI controller including the equations previously proposed is shown in Figure 6.

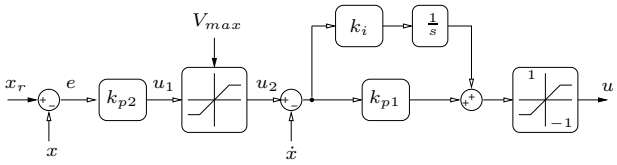

Figure 6: P-PI controller including ARW strategy.

6 Simulation Results

In this section, a simulator and some simulation results are presented to illustrate the performance of ROV based on the complete motion equations. The simulator was implemented using MatLab (The MathWorks, Inc.) and validated by several tests with different initial conditions.

Hydrodynamic, inertial, gravity and buoyancy effects were modeled as shown in (Cunha et al., 1991). However, the weight of umbilical cable and the interference among thrusters were not considered. In order to tune the simulator, the identification of the following parameters are required: mass and volume of the vehicle, inertial moment matrix, gravity and buoyancy centers, additional mass matrix and drag coefficient. Figure 7 shows the time evolution of the yaw angle, when external disturbances (in this case, rectangular pulses) are applied at $t = 15$ [s], $t = 35$ [s] and $t = 90$ [s], including measurement noise. In spite of disturbances acting on the system, the performance of the P-PI control was satisfactory.

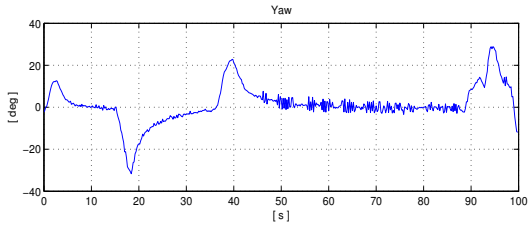

Figure 7: Simulation results of P-PI control under external disturbances: yaw angle.

7 Experimental Results

In this section some results obtained by experimental tests performed with LUMA in the COPPE/LabOceano's ocean basin are presented. The aim of these tests was to verify the ROV operation and to check the performance of the yaw controller.

The controller tunning was performed as in (Cunha et al., 1991), resulting in the following gains: $k_{p1} = 0.025$, $k_i = 0.018$ and $k_{p2} = 0.66$. Figure 8(c) shows the time behavior of the yaw angle under P-PI control during longitudinal and transversal displacements of the ROV for $t \in [0\,,70]$. For $t > 70$ the automatic control was turned off and the command mode was switched to manual mode, reducing the maneuverability of the vehicle. Note that, from Figures 8(a) and 8(b) the roll and pitch angles remain essentially unchanged.

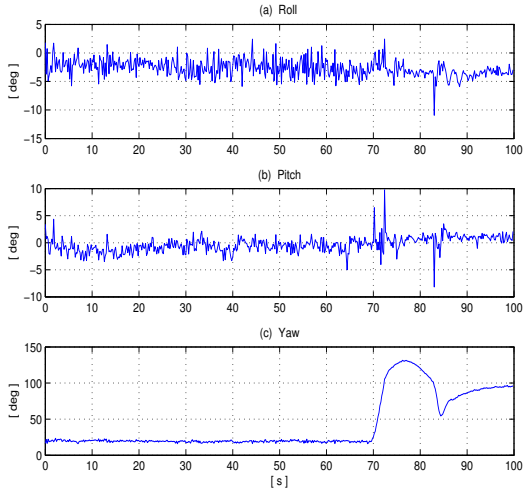

Figure 8: Experimental results of P-PI control: (a) roll, (b) pitch, and (c) yaw angle.

8 Conclusion and Future Works

This work describes the LUMA ROV design concept, its mathematical modeling, simulator implementation, and some details of the heading control design. In order to develop a simulator for the LUMA, a realistic model is considered which includes the thruster dynamics, the gravity and hydrodynamic effects.

As the next step, the design of the depth controller will be considered and new tests using the COPPE/LabOceano's ocean basin facilities will be performed in order to verify the viability of the proposed scheme. Soon, tests will also be performed using hydroacoustic altimeters, currently under development at COPPE/Department of Biomedical Engineering. These sensors will be employed to control the relative distance of the LUMA ROV with respect to the tunnel walls.

Acknowledgment

This work was partly supported by ANEEL/AMPLA, CNPq and FAPERJ.

Figure 9: LUMA in the COPPE/LabOceano's ocean basin.

References

Ageev, M. D., Boreyko, A. A., Gornak, V. E., Matvienko, Yu. V., Scherbatyuk, A. P., Vanlin, Yu. V. and Zolotarev, V. V., (2000). "Modernized TSL-underwater robot for tunnel and shallow-water inspection", in *Int. Symposium on Underwater Technology*, pp. 90–95, Tokyo.

Astrom, K. J and Wittenmark, B., (2003)., Computer-Controlled Systems: Theory and Desing, Prentice-Hall, 3rd Edition, 1997.

Astrom, K. J and Hagglund, T., (1984). "Automatic tuning of simple regulators with specifications on phase and amplitude margins", in *Automatica*, vol. 20, no. 5, pp. 645–651.

Avila, J. P. J., Adamowski, J. C. and Barbarini, L. H. M., (2004). "Estimating the hydrodynamic characteristics of a semi-autonomous underwater vehicle", in *Proc. of the 15th Brazilian Conference on Automatic Control*, Gramado.

Clarke, R., (2002). "An Alternative To Dewatering Pressure Tunnels For Inspection Purposes", in *5th North American Rock Mechanics Symp. and 17th Tunnelling Association of Canada Conf.*, Toronto.

Cunha, J. P. V. S., Dominguez, R. B., Costa, R. R. and Hsu, L., (1991). "Design of a new high performance VS position control of ROVs", in *Proc. Int. Offshore and Polar Eng. Conf.*, Edinburgh.

Ishidera, H., Tsusaka, Y., Ito, Y., Oishi, T., Chiba, S. and Maki, Y., (1986). "Simulation and experiment of automatic controlled ROV", in *Proc. of the 5th Int. Off-shore Mechanical and Artic Eng. Symp.*, pp. 260–267.

Hsu, L., Costa, R. R., Lizarralde, F. and Cunha, J. P. V. S., (1991). "Dynamic positioning of remotely operated underwater vehicles", in *IEEE Robotics & Automation Magazine*, vol. 7, no. 3, pp. 21–31,

Marty, P., (2003). "ALIVE: An autonomous Light Intervention Vehicle", in *Deep Offshore Technology Conf.*, France.

Russel, G. T., (1984). "A design methodology for nonlinear systems", in *S.A. Billings, J. O. Gray and D. H. Owens, eds*, Nonlinear system design, IEEE, chapter 8, pp. 129–144.